Dual-wavelength Bi_2Se_3-based passively Q-switching Nd^{3+}-doped glass all-fiber laser

Xiaofeng Rong (戎小凤)[1,2], Saiyu Luo (罗塞雨)[1], Wensong Li (李文松)[1], Shuisen Jiang (江水森), Xigun Yan (严希滚)[1], Xiaofeng Guan (关小峰)[1], Zhiyong Zhou (周志勇)[1], Bin Xu (徐 斌)[1], Nan Chen (陈 楠)[1], Degui Wang (王德贵)[2], Huiying Xu (许惠英)[1], and Zhiping Cai (蔡志平)[1,*]

[1]*Department of Electronic Engineering, School of Information Science and Engineering, Xiamen University, Xiamen 361005, China*

[2]*School of Physics and Electronic Science, Guizhou Normal University, Guiyang 550001, China*

**Corresponding author: zpcai@xmu.edu.cn*

Received July 29, 2017; accepted September 22, 2017; posted online December 26, 2017

We demonstrate a dual-wavelength passively Q-switched Nd^{3+}-doped glass fiber laser using a few-layer topological insulator Bi_2Se_3 as a saturable absorber (SA) for the first time, to the best of our knowledge. The laser resonator is a simple and compact linear cavity using two fiber end-facet mirrors. The SA is fabricated by Bi_2Se_3/polyvinyl alcohol composite film. By inserting the SA into the laser cavity, a stable Q-switching operation is achieved with the shortest pulse width and maximum pulse repetition rate of 601 ns and 205.2 kHz, respectively. The maximum average output power and maximum pulse energy obtained are about 6.6 mW and 38.8 nJ, respectively.

OCIS codes: 060.3510, 140.3540, 140.3530, 160.4236.
doi: 10.3788/COL201816.020016.

Dual-wavelength Q-switching (QS) fiber lasers have attracted great attention because of their practical applications in medicine, biomedical imaging, and terahertz technology[1–4]. Compared to actively QS fiber lasers, passively QS fiber lasers possess the attractive advantages of compactness, simplicity, and flexibility. With the assistance of the saturable absorbers (SAs), passively QS pulses can be generated in fiber lasers[5–8]. Moreover, all-fiber laser sources hold considerable research interest owing to their compact, convenient, and cost-effective designs. Nd^{3+}-ion-based laser materials own an evident multi-peak structure of an emission spectrum and a relatively high gain at an ~1 μm waveband, where the lasing could be more easily realized in a suitable laser cavity design[9]. A common 1064 nm lasing based on Nd^{3+}-doped laser materials has been mainly studied in bulk solid-state lasers, however, there is no report to date existing for an all-fiber laser configuration.

Two-dimensional (2D) materials as SAs have attracted great attention in recent years, which include graphene[10–16], topological insulators (TIs)[17–21], transition-metal dichalcogenides (TMDs)[22–25], and black phosphorus[26–28]. Take the TIs as an example, e.g., Bi_2Se_3, have been reported as effective SA for pulsed fiber laser operation and showed a broadband saturable absorption[18,29]. Recently, Luo *et al.* reported the first 1.06 μm QS ytterbium-doped fiber laser using Bi_2Se_3 as an SA, which obtained maximum pulse energy of 17.9 nJ and pulse repetition rate ranging from 8.3 to 29.1 kHz[18]. A Bi_2Se_3-based 604 nm passively QS praseodymium laser has been demonstrated with pulse trains ranging from 86.2 to 187.4 kHz[29]. Moreover, in the past few years, several research works have been reported on the use of 2D materials as SAs for achieving simultaneous dual-wavelength pulse generation[5,30]. For example, Guo *et al.* reported the dual-wavelength soliton pulses with the WS_2-based fiber taper, and the pulses width are ~585 and ~605 fs, respectively[30]. Luo *et al.* demonstrate a Q-switched dual-wavelength erbium-doped fiber laser based on graphene as an SA[5].

In this work, we experimentally demonstrate a compact dual-wavelength passively Q-switched Nd^{3+}-doped glass all-fiber laser at 1065.8 and 1074.3 nm for the first time, to the best of our knowledge. A few-layer Bi_2Se_3/polyvinyl alcohol (PVA) film inserted into a fiber connector constructed the effective SA. Stable pulse trains were attained with the repetition rate range of 69.68–205.2 kHz with the pulse width varying from 1.42 to 0.601 μs. The achieved maximum pulse energy and maximum average output power are 38.83 nJ and 6.5 mW, respectively.

High-quality Bi_2Se_3 films were produced by a liquid-phase exfoliation method[29]. Figure 1 depicts the features of the as-arranged TI Bi_2Se_3. The bulk Bi_2Se_3 and the as-arranged few-layer Bi_2Se_3 are both distinguished by X-ray diffraction (XRD) in Fig. 1(a), where all the marked spikes of the bulk Bi_2Se_3 can be readily listed to rhombohedral Bi_2Se_3 (JCPDs No. 89-2008). The bulk Bi_2Se_3 had been satisfactorily scaling off because the XRD arrangement of the few-layer Bi_2Se_3 exhibits a high direction, as well as certain featured spikes vanished[31]. Both few-layer Bi_2Se_3 and bulk Bi_2Se_3 were numerically distinguished by the Raman scope, as shown in Fig. 1(b). It is apparent that the few-layer Bi_2Se_3 displays an apparent change of spike, and its featured spikes are at 72, 128, and 172 cm^{-1}. Moreover, the average denseness of the height profile

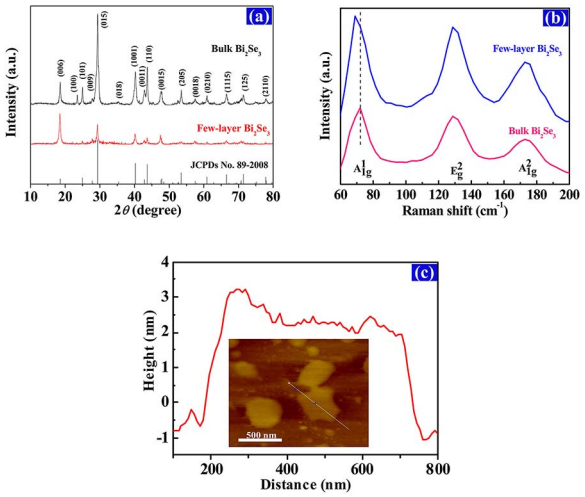

Fig. 1. (Color online) (a) XRD and (b) Raman spectrum of bulk Bi_2Se_3 and few-layer Bi_2Se_3, (c) height profile of an as-arranged few-layer Bi_2Se_3 sample. Inset: AFM image.

chart inset in Fig. 1(c) was found to be ~4 nm, showing that the as-arranged Bi_2Se_3 nanosheets are approximately three to four layers, since the denseness of a single-layer Bi_2Se_3 is 0.96 nm[29]. The denseness of the as-arranged few-layer Bi_2Se_3 was studied by atomic force microscopy (AFM), as depicted in Fig. 1(c). To help with the real-life usage, we separated the few-layer Bi_2Se_3 mixture into the PVA for film formation[18].

Like graphene, Bi_2Se_3 is also a Dirac substance with a unique Dirac cone on the surface close to the Γ point[32]. Particularly, Bi_2Se_3 boasts the topologically significant energy gaps as confined as ~0.3 eV[33], thus the ultra-broadband saturable soaking-up may occur with the aid of Pauli-blocking influence (similar to graphene)[34]. With Bi_2Se_3 as an example, its saturable soaking-up wavelength scope can allow from viewable to mid-infrared[35]. Consequently, those obtained outcomes on the TI's visual optical absorption manifest that the few-layer TI as a SA might be preferable for creating QS or mode-locked lasers.

The experimental setup of the proposed Bi_2Se_3-based passively QS Nd^{3+}-doped glass all-fiber laser is shown in Fig. 2(a). The laser resonator was a simple and compact linear cavity with a cavity length of about 2.7 m. It consists of an 808 nm laser diode (LD), an Nd^{3+}-doped glass fiber, and a pair of fiber end coating mirrors. A piece of free-standing Bi_2Se_3/PVA film was sandwiched between two fiber ferrules to construct a fiber compatible SA. Then, the Bi_2Se_3-SA was incorporated into the laser cavity, acting as a Q-switcher. The pump source was based on an 808 nm fiber-coupled diode laser (core/cladding, 8.2/125 μm; 0–250 mW). A 2.35-m-long Nd^{3+}-doped glass fiber was used as the gain medium, and the absorption coefficient was calculated to be about 8.36 dB/m at the pumping wavelength. The all-fiber laser oscillation was constructed by a pair of homemade fiber end-facet mirrors M1 and M2. Both mirrors were fabricated by coating SiO_2/Ta_2O_5 dielectric film onto fiber ferrules of the

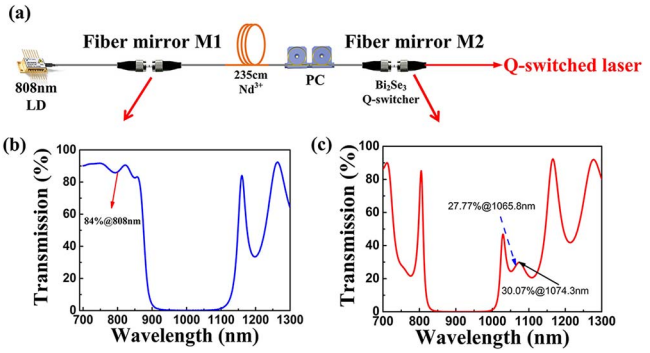

Fig. 2. (a) Schematic of the laser experimental setup of Nd^{3+} glass passively QS, transmission curves of the fiber mirror (b) M1 and (c) M2.

SMF-28e using a plasma sputter deposition system (SCTS500, System Control Technologies, Inc.). As shown in Fig. 2(b), input mirror M1 has a high transmittance of 84% at 808 nm and a high reflectivity in the vicinity of 1 μm. Output mirror M2 is shown in Fig. 2(c) and characterized by the transmittances of 27.77% and 30.07% at 1065.8 and 1074.3 nm, respectively. According to the emission spectrum of the Nd^{3+}-doped glass fiber, the cavity gain competition finally leads to the 1065.8 and 1074.3 nm lasing. Here, a polarization controller (PC) is used to properly adjust for optimizing the QS operation.

Figure 3 shows the output power characteristics in continuous-wave (CW) and QS regimes. The output power was measured by a power meter (Coherent PM3). The threshold of pump power for CW operation is about 6 mW. By increasing the pump power, the CW maximum output power obtained was 37.78 mW, corresponding to a slope efficiency of about 14.74%. Here, due to the lack of an optical modulator in the cavity, only CW operation was observed from the oscilloscope, even with changing the pump power or manipulating the PC, which excluded the possibility of self-pulsing. When the Bi_2Se_3-SA was inserted into the laser cavity, the QS pulses initiated at the pump power of 50 mW, and stable QS pulses were obtained at the pump power of 70 mW. The maximum

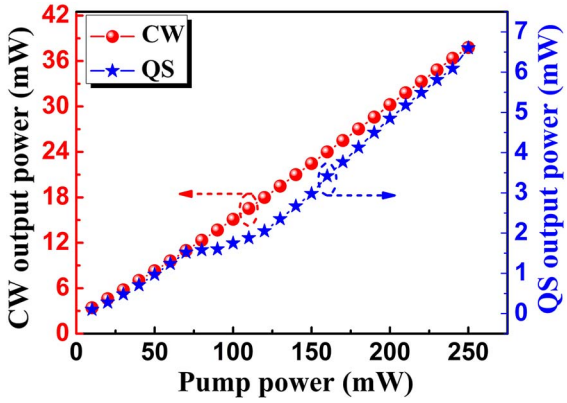

Fig. 3. (Color online) Output powers as a function of pump powers in CW and QS regimes.

average output power of the stable QS all-fiber laser was 6.6 mW, and the slope efficiency was 2.75%.

Figure 4 shows the optical spectra of the proposed dual-wavelength all-fiber laser in CW and QS operations, respectively, which were measured by a Hewlett Packard 70004A optical spectrum analyzer (OSA) at the pump power of 70 mW. Figure 4(a) shows the typical characteristic of the CW operation with the lasing peaks at 1065.3, 1073.4, and 1080.3 nm, respectively. At the available pump power level, the CW lasing wavelength was unstable, either with two lasing peaks at 1065.3 and 1073.4 nm or three lasing peaks, as mentioned above. This feature is attributed to the competition between gain and loss at different levels. As shown in Fig. 5(b), for QS operation, the effective competition between gain and loss leading to the dual-wavelength of both 1065.8 and 1074.3 nm lasing and the corresponding 3 dB bandwidth are measured to be 1.82 and 1.75 nm, respectively, whereas the QS lasing state always kept stable dual-wavelength operation at both 1065.8 and 1074.3 nm.

Furthermore, we exhibit the typical pulse trains of the QS all-fiber laser, as given in Fig. 5, which were recorded by a photo detector (DET10A, Thorlabs, 600–1700 nm) and a 200 MHz bandwidth and 1 Gs/s sampling rate digital oscilloscope (Hantek, DSO5202P). When the pump power was gradually increased from 80 to 240 mW, stable pulse trains with different repetition rates were observed at four different pump powers of 80, 140, 170, and 240 mW. As we can see from Fig. 5(a), at the pump power of 80 mW, the repetition rate was about 91.58 kHz. When the pump power was increased to 140 mW, the repetition rate was 111.9 kHz [see Fig. 5(b)]. By further increasing the pump power to 170 mW, the repetition rate increased to about 131.1 kHz [see Fig. 5(c)]. Finally, when the pump power reached 240 mW, the repetition rate increased to 194 kHz with a slight pulse intensity fluctuation [see Fig. 5(d)].

When the pump power was 140 mW, a single pulse time duration of 0.878 μs (i.e., 878 ns) was depicted in Fig. 6(a), where inset is the corresponding pulse train. In order to evaluate the proposed dual-wavelength all-fiber laser, we measured the radio-frequency (RF) spectrum using an RF spectrum analyzer (Gwinstek GSP-930) at the resolution bandwidth (RBW) of 30 Hz. As shown in Fig. 6(b), a signal-to-noise ratio (SNR) of ~43 dB, corresponding to the fundamental frequency of 111.9 kHz at the pump power of 140 mW, was recorded. Meanwhile, aside from tenth-order harmonic frequencies, the broadband RF is regular with no other modulated components. These results verify the good QS stability.

Finally, Fig. 7(a) shows the evolution of the pulse repetition rate and the pulse duration with the pump power. By increasing the pump power, the pulse repetition rate varied from 69.68 to 205.2 kHz, while the pulse duration was narrowed from 1.42 to 0.601 μs. This is a typical

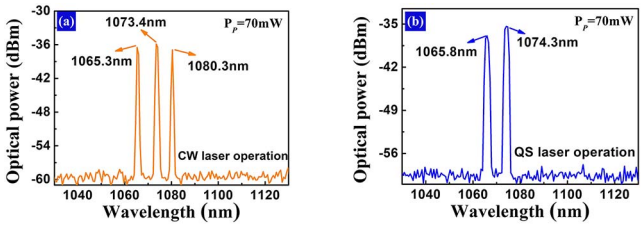

Fig. 4. Output optical spectra of dual-wavelength all-fiber laser at 1065.8 and 1074.3 nm, operating in (a) CW and (b) QS regime, respectively.

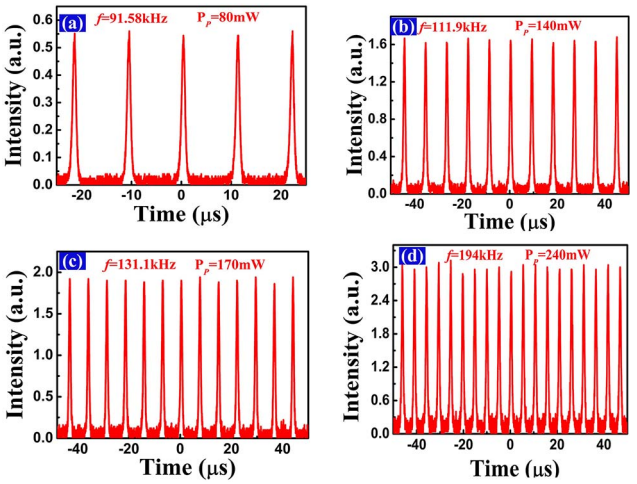

Fig. 5. Output pulse trains under different pump powers at (a) $P_P = 80$, (b) $P_P = 140$, (c) $P_P = 170$, and (d) $P_P = 240$ mW.

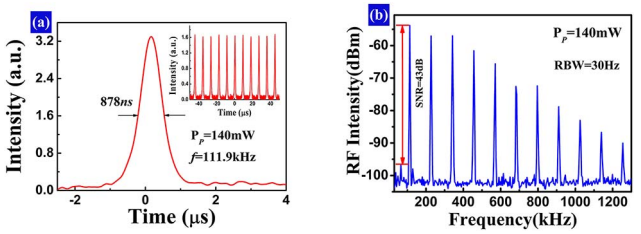

Fig. 6. The pump power at 140 mW of (a) single pulse time duration of a QS laser. Inset: QS pulse trains at a same pump power. (b) RF output spectrum.

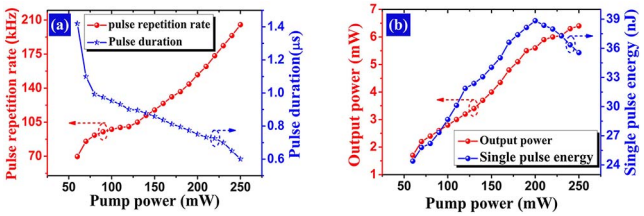

Fig. 7. (Color online) (a) Repetition rate and the pulse duration as a function of the pump power. (b) The output power and the pulse energy as a function of the pump power.

passively Q-switched feature[36,37]. The shortest pulse duration is 0.601 μs (i.e., 601 ns), which could be further shortened using a shorter cavity length. Moreover, we measured the variations of the output power and the pulse energy with the pump power, as shown in Fig. 7(b). By increasing the pump power from 70 to 250 mW, the output power increased from 0.9 to 6.6 mW and the pulse energy increased from 24.3 to 38.8 nJ, correspondingly. The pulse energy showed good linearity between 70 and 210 mW. However, it showed an obvious saturation effect as the pump power exceeded 210 mW. We consider that this is most probably due to the thermal accumulation of the Bi_2Se_3-SA in the case of higher pump power, which results in the bleaching effects. Herein, to exclude the thermal damage of the Bi_2Se_3-SA, we repeatedly implemented the pump power increase from 0 to 250 mW and decreased it back several times. During the whole process, stable QS operation was still observed, demonstrating that the Bi_2Se_3-SA was not damaged.

In conclusion, we experimentally demonstrate a compact Bi_2Se_3-based dual-wavelength passively Q-switched all-fiber laser operating at 1065.8 and 1074.3 nm. Using an 808 nm LD as the pump source, the linear all-fiber laser cavity is simply fabricated by a 2.35-m-long Nd^{3+}-doped fiber and two fiber end-facet mirrors. The CW laser is obtained with a maximum output power of 37 mW, and the QS laser has a maximum average output power of 6.6 mW. The stable QS operation is characterized by the maximum pulse energy of 38.83 nJ and the shortest pulse duration of 601 ns, corresponding to the pulse repetition rate ranging from 69.68 to 205.2 kHz. We believe that the proposed dual-wavelength passively Q-switched laser could be suitable for practical applications, such as optical communication, optical sensors, and terahertz technology.

This work was supported by the National Natural Science Foundation of China (NSFC) (No. 61275050), the Project funded by the Department of Education of Guizhou Province (No. [2016]140), the Science and Technology Foundation of Guizhou Province (Nos. [2014] 2124, [2010]2146, and [2009]06), the Science and Technology Plan Projects of Guizhou Province (No. SY2013 [3055]), the Science-Technology Union Foundation of Guizhou Province (No. [2014]7045), and the International Science-Technology cooperation project of Guizhou Province of China (No. [2013]7019).

References

1. U. Keller, Nature **424**, 831 (2003).
2. Z. P. Sun, A. Martinez, and F. Wang, Nat. Photon. **10**, 227 (2016).
3. R. M. Sova, C.-S. Kim, and J. U. Kang, IEEE Photon. Technol. Lett. **14**, 287 (2002).
4. B. M. Walsh, Laser. Phys. **20**, 622 (2010).
5. Z. Q. Luo, M. Zhou, J. Weng, G. M. Huang, H. Y. Xu, C. C. Ye, and Z. P. Cai, Opt. Lett. **35**, 3709 (2010).
6. W. S. Li, T. J. Du, J. L. Lan, C. L. Guo, Y. J. Cheng, H. Y. Xu, C. H. Zhu, F. Q. Wang, Z. Q. Luo, and Z. P. Cai, Opt. Lett. **42**, 671 (2017).
7. T. Du, Z. Luo, R. Yang, Y. Huang, Q. Ruan, Z. Cai, and H. Xu, Opt. Lett. **42**, 462 (2017).
8. H. Ahmad, M. A. M. Salim, Z. A. Ali, M. F. Ismail, K. Thambiratnam, A. A. Latif, N. Nayan, and S. W. Harun, Chin. Opt. Lett. **14**, 091403 (2016).
9. H. F. Lin, W. Z. Zhu, F. B. Xiong, and J. J. Ruan, App. Opt. **56**, 948 (2017).
10. H. Yang, X. Feng, Q. Wang, H. Huang, W. Chen, A. T. Wee, and W. Ji, Nano. Lett. **11**, 2622 (2011).
11. Z. Sun, T. Hasan, F. Torrisi, D. Popa, G. Privitera, F. Wang, F. Bonaccorso, D. M. Basko, and A. C. Ferrari, ACS Nano. **4**, 803 (2010).
12. Y. Fujimoto, T. Suzuki, R. A. M. Ochante, T. Hirayama, M. Murakami, H. Shiraga, M. Yoshida, O. Ishii, and M. Yamazaki, Electron. Lett. **50**, 1470 (2014).
13. Y. F. Song, L. Li, D. Y. Tang, and D. Y. Shen, Laser Phys. Lett. **10**, 125103 (2013).
14. H. Zhang, D. Y. Tang, R. J. Knize, L. M. Zhao, and Q. L. Bao, Appl. Phys. Lett. **96**, 111112 (2010).
15. Y. F. Song, L. Li, H. Zhang, D. Y. Shen, D. Y. Tang, and K. P. Loh, Opt. Express. **21**, 10010 (2013).
16. Y. F. Song, H. Zhang, D. Y. Tang, and D. Y. Shen, Opt. Express **20**, 27283 (2012).
17. B. Chen, X. Zhang, K. Wu, H. Wang, J. Wang, and J. Chen, Opt. Express **23**, 26723 (2015).
18. Z. Q. Luo, Y. Z. Huang, J. Weng, H. H. Cheng, Z. Q. Lin, B. Xu, Z. P. Cai, and H. Y. Xu, Opt. Express **21**, 29516 (2013).
19. D. D. Wu, Z. P. Cai, Y. L. Zhong, J. Peng, J. Weng, Z. Q. Luo, N. Chen, and H. Y. Xu, IEEE Photon. Technol. Lett. **27**, 379 (2015).
20. Y. Huang, Z. Luo, Y. Li, M. Zhong, B. Xu, K. Che, H. Xu, Z. Cai, J. Peng, and J. Weng, Opt. Express **22**, 25258 (2014).
21. H. J. Zhang, C. X. Liu, X. L. Qi, X. Dai, Z. Fang, and S. C. Zhang, Nat. Phys. **5**, 438 (2009).
22. W. S. Li, J. Peng, Y. L. Zhong, D. D. Wu, H. Y. Lin, Y. J. Cheng, Z. Q. Luo, J. Weng, H. Y. Xu, and Z. P. Cai, Opt. Mater. Express **6**, 2031 (2016).
23. B. Lu, L. Yuan, X. Qi, L. Hou, B. Sun, P. Fu, and J. Bai, Chin. Opt. Lett. **14**, 071404 (2016).
24. H. Zhang, S. B. Lu, J. Zheng, J. Du, S. C. Wen, D. Y. Tang, and K. P. Loh, Opt. Express **22**, 7249 (2014).
25. X. Zou, Y. Leng, Y. Li, Y. Feng, P. Zhang, Y. Hang, and J. Wang, Chin. Opt. Lett. **13**, 081405 (2015).
26. R. Zhang, Y. Zhang, H. Yu, H. Zhang, R. Yang, B. Yang, Z. Liu, and J. Wang, arXiv **1505**, 05992 (2015).
27. Z. Luo, M. Liu, Z. Guo, X. Jiang, A. Luo, C. Zhao, X. Yu, W. Xu, and H. Zhang, Opt. Express **23**, 20030 (2015).
28. Z. P. Qin, G. Q. Xie, H. Zhang, C. J. Zhao, P. Yuan, S. C. Wen, and L. J. Qian, Opt. Express **23**, 24713 (2015).
29. H. Y. Lin, W. S. Li, J. L. Lan, X. F. Guan, H. Y. Xu, and Z. P. Cai, App. Opt. **56**, 802 (2017).
30. B. Guo, Y. Yao, P. G. Yan, K. Xu, J. J. Liu, S. G. Wang, and Y. Li, IEEE Photon. Technol. Lett. **28**, 323 (2016).
31. B. Xu, Y. Wang, J. Peng, Z. Q. Luo, H. Y. Xu, Z. P. Cai, and J. Weng, Opt. Express **23**, 7674 (2015).
32. J. N. Coleman, M. Lotya, A. O'Neill, S. D. Bergin, P. J. King, U. Khan, K. Young, A. Gaucher, S. De, R. J. Smith, I. V. Shvets, S. K. Arora, G. Stanton, H.-Y. Kim, K. Lee, G. T. Kim, G. S. Duesberg, T. Hallam, J. J. Boland, J. J. Wang, J. F. Donegan, J. C. Grunlan, G. Moriarty, A. Shmeliov, R. J. Nicholls, J. M. Perkins, E. M. Grieveson, K. Theuwissen, D. W. McComb, P. D. Nellist, and V. Nicolosi, Science **331**, 568 (2011).
33. H. Zhang, C. X. Liu, X. L. Qi, X. Dai, Z. Fang, and S. C. Zhang, Nat. Phys. **5**, 438 (2009).

34. Z. Q. Luo, C. L, Y. Z. Huang, D. D. Wu, J. Y. Wu, H. Y. Xu, Z. P. Cai, Z. Q. Lin, L. P. Sun, and J. Weng, IEEE J. Sel. Top. Quantum Electron. **20**, 0902708 (2014).
35. B. Braun, F. X. Kartner, G. Zhang, M. Moser, and U. Keller, Opt. Lett. **22**, 381 (1997).
36. E. J. R. Kelleher, J. C. Travers, Z. P. Sun, A. G. Rozhin, A. C. Ferrari, S. V. Popov, and J. R. Taylor, Appl. Phys. Lett. **95**, 111108 (2009).
37. J. Liu, S. Wu, Q. H. Yang, and P. Wang, Opt. Lett. **36**, 4008 (2011).